THE JOURNAL OF BIOLOGICAL CHEMISTRY
Vol. 280, No. 15, Issue of April 15, pp. 15279–15288, 2005
Printed in U.S.A.
© 2005 by The American Society for Biochemistry and Molecular Biology, Inc.

Role of Arginine 220 in the Oxygen Sensor FixL from *Bradyrhizobium japonicum**[S]

Received for publication, December 10, 2004, and in revised form, January 25, 2005
Published, JBC Papers in Press, February 11, 2005, DOI 10.1074/jbc.M413928200

Véronique Balland‡, Latifa Bouzhir-Sima§, Laurent Kiger¶, Michael C. Marden¶, Marten H. Vos§, Ursula Liebl§, and Tony A. Mattioli‡‖

From the ‡Laboratoire de Biophysique du Stress Oxydant, SBE/DBJC and CNRS URA 2096, CEA/Saclay, 91191 Gif-sur-Yvette cedex, France, the §Laboratoire d'Optique et Biosciences, INSERM U451, CNRS UMR 7645, Ecole Polytechnique-ENSTA, 91128 Palaiseau, France, and ¶INSERM Unité 473, 78, rue du Général Leclerc, 94275 Le Kremlin-Bicêtre, France

In the heme-based oxygen sensor protein FixL, conformational changes induced by oxygen binding to the heme sensor domain regulate the activity of a neighboring histidine kinase, eventually restricting expression of specific genes to hypoxic conditions. The conserved arginine 220 residue is suggested to play a key role in the signal transduction mechanism. To obtain detailed insights into the role of this residue, we replaced Arg^{220} by histidine (R220H), glutamine (R220Q), glutamate (R220E), and isoleucine (R220I) in the heme domain FixLH from *Bradyrhizobium japonicum*. These mutations resulted in dramatic changes in the O_2 affinity with K_d values in the order R220I < R220Q < wild type < R220H. For the R220H and R220Q mutants, residue 220 interacts with the bound O_2 or CO ligands, as seen by resonance Raman spectroscopy. For the oxy-adducts, this H-bond modifies the π acidity of the O_2 ligand, and its strength is correlated with the back-bonding-sensitive ν_4 frequency, the k_{off} value for O_2 dissociation, and heme core-size conformational changes. This effect is especially strong for the wild-type protein where Arg^{220} is, in addition, positively charged. These observations strongly suggest that neither strong ligand fixation nor the displacement of residue 220 into the heme distal pocket are solely responsible for the reported heme conformational changes associated with kinase activity regulation, but that a significant decrease of the heme π^* electron density because of strong back-bonding toward the oxygen ligand also plays a key role.

Oxygen regulates diverse processes essential to life and has recently been identified as an activity regulator ligand for several heme-based sensor proteins, with either histidine kinase activity as for FixL in *Rhizobia,* or phosphodiesterase activity as for *Ec*DOS[1] in *Escherichia coli* and PDEA1 in *Acetobacter* (1, 2, 3). Heme-based sensors carry out crucial roles in biological signaling in prokaryotic and eukaryotic organisms responding to various gaseous ligands such as dioxygen, nitric oxide (guanylate cyclase, Ref. 4), or carbon monoxide (CooA, a CO-sensing protein of *Rhodospirillum rubrum*, Refs. 5 and 6; NPAS2, Ref. 7). In these sensor proteins, the heme cofactor plays a central role not only in binding the respective effector molecules but also in regulating the associated enzymatic function via heme and protein conformational changes induced by ligand binding. The N-terminal segments of several of these proteins (FixL, *Ec*DOS, PDEA1, and NPAS2) consist of a heme sensor domain whose fold characterizes them as PAS domains. These domains are proposed to share a common conformational flexibility, potentially related to a mechanism for communicating ligand binding and signal transduction (8). PAS domains were also identified in several non-heme proteins involved in the mammalian oxygen-sensing pathway, as ARNT or HIF1-α, which play crucial roles in the cellular metabolic changes under hypoxic conditions (9).

The FixL/FixJ two-component regulatory system is part of the signaling cascade of *Bradyrhizobium japonicum* that enables this bacterium to adapt its respiratory energy metabolism to the microaerobic environment during root hair invasion and nodule formation (10). The FixL proteins have a histidine kinase domain, responsible for the phosphorylation of the transcription factor FixJ, and an oxygen-sensing heme domain (11). Similar to the oxygen storage protein myoglobin, the heme domain has a *b*-type heme as prosthetic group with a proximal histidine as axial ligand. Both the deoxy-Fe^{II} and Met-Fe^{III} forms are high spin and 5-coordinated (12). Upon oxygen fixation, the heme becomes low spin 6-coordinated, and the kinase activity strongly diminishes. Thus, a local perturbation at the heme domain is transduced over a relatively long distance within the protein. Diminished kinase activity has also been observed with low spin CO or NO adducts, but to a far lesser degree (13, 14). Therefore, it is not solely the spin change of the heme upon ligand binding that is responsible for the switching of the kinase activity.

Structural studies indicate similarities in the steady-state heme geometry of the oxy-complexes of FixLH and Mb proteins (15), as well as in the bond strength between the heme iron and O_2 (16). However, notable differences are observed, especially with regard to the dynamic aspects of the interaction with oxygen. Oxygen affinity is much lower in FixL (17), whereas oxygen geminate recombination after O_2 dissociation occurs with unprecedented efficiency and high yield (18). Thus, unlike myoglobin, there is substantial reorganization in the FixL heme pocket upon O_2 fixation that acts as an oxygen trap, a finding consistent with the x-ray crystallo-

* This work was supported in part by the Regional Council of the Ile-de-France (to T. A. M.). The costs of publication of this article were defrayed in part by the payment of page charges. This article must therefore be hereby marked "*advertisement*" in accordance with 18 U.S.C. Section 1734 solely to indicate this fact.

[S] The on-line version of this article (available at http://www.jbc.org) contains Supplemental Materials.

‖ To whom correspondence should be addressed: Service de Bioénergétique, Département de Biologie Joliot-Curie, CEA Saclay, F-91191, Gif-sur-Yvette Cedex, France. Tel.: 33-169-08-41-66; Fax: 33-169-08-87-17; E-mail: tony.mattioli@cea.fr.

[1] The abbreviations used are: *Ec*DOS, direct oxygen sensor from *E. coli*; *Bj, B. japonicum*; FixL*, soluble truncated FixL; FixLH, heme domain of FixL; FG loop, Thr^{209} to His^{220} in *Bj*FixLH; Hb, hemoglobin; HS, high spin; LS, low spin; Mb, myoglobin; RR, resonance Raman; *SW,* sperm whale; WT, wild type; FT-IR, Fourier transform infrared.

This is an Open Access article under the CC BY license.

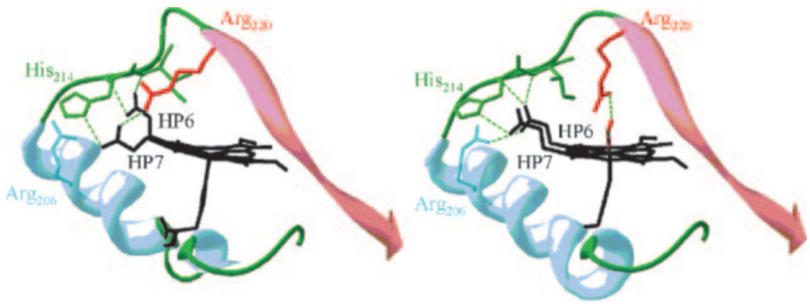

FIG. 1. **Crystallographic structures of the deoxy (*left*, PDB entry 1LSW, Ref. 20) and oxy (*right*, PDB entry 1DP6, Ref. 15) states of *Bj*FixLH.** Arg^{220} and β-sheets are in *red*, Arg^{206} and α-helix in *cyan*, His^{214} and Ile^{215} and loops are represented in *green*. The heme-propionate 6 and 7 are labeled *HP6* and *HP7*, respectively.

graphic structures of the heme domain obtained for *Bj*FixL (*Bj*FixLH) (15, 19, 20). Upon O_2 or CN^- binding, the FixL heme pocket structure is significantly modified, especially the position of the FG loop (Thr^{209} to Arg^{220}), and the spatial position of one arginine (Arg^{220}) moves from the propionate 7 group of the heme toward the oxygen ligand (Fig. 1). Based on these structures, the mechanism of primary signal transduction has been suggested to involve the heme propionates and two arginine residues (Arg^{206} and Arg^{220}). One model proposes that flattening of the heme plane upon ligand binding leads to a shift in the position of the heme propionates reducing the strength of the salt bridge between Arg^{220} and propionate 7 (15). As a result, the arginine at position 220 shifts into the distal pocket of FixL where a H-bond can be formed with the ligand (O_2, CN^-), leading to new polar interactions and eventually inducing the structural reorganization responsible for kinase inactivation (20). Movement in the FG loop is thus thought to be an important element of this structural reorganization responsible for kinase inactivation.

Recently, the three-dimensional crystallographic structure of the R220A mutant of *Bj*FixLH in its Fe^{III} state has been described (14). Inhibition of the histidine kinase activity was strongly affected by this mutation as reported for the cyanomet-FixL adduct, but it was not reported for the oxy form because binding of O_2 was very inefficient (K_d = 1500 μM^{-1}). According to the description of the Fe^{III} R220A mutant structure, the major structural modifications involved the heme planarity, the lengthening of the axial Fe^{III}-N_{His} bond, and the propionate 7 geometry.

Arg^{220} is a conserved residue among all known FixL proteins, and its equivalent is also found in the distal pocket of the *Ec*DOS sensor protein (Arg^{64}) (21). The x-ray structures of *Bj*FixLH as well as *Ec*DOSH point to the importance of this residue, which interacts with the bound O_2 ligand, but its exact role in the O_2 affinity and chemical details related to Fe-O_2 adduct stabilization are not clear. Here, we have constructed four site-directed mutants of *Bj*FixLH at position 220 to study the influence of Arg^{220} on the heme conformation and on the nature of O_2 binding. The point mutations were chosen in order to modify the electrostatic properties and H-bonding capabilities of residue 220, with minor steric modifications of the side chain. Therefore, Arg^{220} was substituted by Ile, Gln, His, and Glu. In this study we use resonance Raman spectroscopy to obtain detailed insight in the structural and electrostatic role of Arg^{220} in different ligation states. In particular, we focus on the oxy-Fe^{II}-O_2 and the Fe^{II}-CO states, because both species exhibit a low-spin 6-coordinated iron with two different heme pockets. The structural information obtained for these states, in terms of residue 220 interactions with bound ligand, can be related to the measured association and dissociation rates for O_2 and CO binding, providing new insights into the factors responsible of the structural reorganization in the FixL sensor and the related function.

MATERIALS AND METHODS

DNA Manipulations, Protein Expression, and Purification—A recombinant gene fragment, corresponding to the region between codons 142 and 270 and encoding the FixL heme domain in *B. japonicum,* was used as template for site-directed mutagenesis reactions. The substitutions R220H, R220Q, R220I, R220A[2] and R220E were introduced following the QuikChange site-directed mutagenesis protocol (Stratagene) by replacing the codon CGC by CAC, CAG, ATC, GCC[2] and GAG, respectively. All constructs were confirmed by DNA sequencing prior to further analyses. The final constructs, containing *fixLH* in the vector pET 28a were transformed into *Escherichia coli* strain BL21 DE3 for expression. Protein expression and purification were performed as described in Liebl *et al.* (18).

Sample Preparation—All protein samples were prepared in 50 mM Tris-HCl buffer at pH 7.4. The deoxy form of *Bj*FixLH was prepared by reduction in deoxygenated buffer, by addition of freshly prepared degassed sodium dithionite (200 μM final concentration) (Sigma) stock solution in deionized water. Except for the Met forms, all modifications of the sample atmosphere were prepared on a system equipped with a vacuum line. These samples were anaerobically sealed with gas-tight rubber septums and transferred, when required, using gas-tight syringes (Hamilton). The O_2 complexes were prepared by addition of an anaerobic sodium ascorbate (Fluka) solution, incubated for 5 min for WT, 15 min for R220Q and R220H, and 30 min for R220I, then flushed with 1 atm O_2 for 30 s. For the $^{18}O_2$ complexes, the flushing was done with $^{18}O_2$ (Eurisotop; 93.3% ^{18}O (atom percent)). The CO complexes were prepared by reduction with excess sodium ascorbate under 1 atm CO. Hydrogen/deuterium exchange experiments were performed by diluting a 50 μM protein sample into a D_2O (Sigma) Tris-DCl buffer solution (pD = 7.4) by a factor of 100. The solution was left for the exchange for 24 h at 4 °C and then concentrated to a final concentration of 30 μM.

UV-Visible Absorption Spectroscopy—Optical absorbance measurements were made using a UVIKON 922 (Kontron) spectrophotometer with a 70-μl airtight quartz cell (Hellma) with a pathlength of 1 cm. Protein concentration was 20 μM, and the measurements were performed at ambient temperature.

Ligand Association—The rates of association (k_{on}) of the FixL proteins with CO or O_2 (except for the oxy-adduct of the R220E mutant), were obtained after flash photolysis with a 10-ns 160-mJ pulse at 532 nm (Quantel YAG laser, France). The heme proteins (10 μM, in 50 mM Tris-HCl buffer, pH 7.4, at 25 °C in 4-mm cuvettes) were reduced with dithionite and equilibrated with CO to form the stable Fe^{II}-CO adduct. The samples were then flushed with air, 1 atm of O_2 or CO (1, 10, and 100%). A typical kinetic curve was obtained averaging a minimum of 5 measurements, with at least 5 s between photolysis pulses to allow sample recovery.

Ligand Dissociation—For all mutants, the rate of O_2 dissociation (k_{off}) was measured according to the method previously described (17, 22). The proteins were equilibrated with a mixture of O_2 and CO (final concentrations of 75 μM CO and 1.3 mM O_2). After photodissociation of the CO, O_2 may rebind to the exposed heme, followed by the replace-

[2] The R220A FixLH mutant has been constructed and characterized by UV-visible spectroscopy and only used for the ligand binding experiments. It was not initially the purpose of this work to study this mutant because we first selected the mutations that would least modify the size of the residue 220 side chain. We observed similar behavior for the R220A and R220E FixLH mutants, with low conversion to the oxy form and rapid degradation of this complex. Thus, the flash photolysis experiments were performed with the R220A mutant as described for the R220E mutant (see "Materials and Methods").

ment of O_2 by CO. If the gas mixture contains nonsaturating amounts of O_2, the P_{50} can be estimated from the fraction that binds after photodissociation of the CO. For the R220E mutant, where autooxidation of the protein may be a problem, this method was used to estimate the k_{on} value for O_2 binding, because the heme was exposed to O_2 for less than 1 s.

FT-IR Spectroscopy—FT-IR spectra were recorded with an IFS 66 (Bruker) spectrometer equipped with a DTGS detector. ATR spectra were taken using a ZnSe reflection crystal (Pike Technologies). 10 μl of the sample solution (0.5 mM) was deposited on the crystal and dried by a gentle stream of nitrogen gas to avoid water contributions to the FT-IR spectra. Reported spectra were the result of the averaging of 10 single spectra recorded with 250 scans. Spectral resolution was 4 cm^{-1}. Baseline corrections were performed using GRAMS 32 software (Galactic Industries).

Resonance Raman Spectroscopy—Resonance Raman spectra were recorded using a modified single-stage spectrometer T64000 (Jobin-Yvon) equipped with a liquid nitrogen-cooled back-thinned CCD detector and 1800 grooves/mm holographic gratings. Samples for the resonance Raman measurements were prepared at a protein concentration of 20 μM. The excitation wavelength at 413.1 nm was provided by a Kr^+ ion laser (Spectra physics series 2000). A 90° scattering geometry was used and laser power at the sample was 5 milliwatt. Holographic notch filters (Kaiser) were placed at the entrance slits (100 μm) to reject stray light. For measurements of the CO derivatives, the laser power was decreased to ≤2 milliwatt to minimize photodissociation using neutral density filters. All spectra were recorded at room temperature using a spinning cell (diameter 2 mm) to prevent excessive photodissociation and avoid local thermal degradation of the protein during the measurements. To accurately determine isotope shifts, the monochromator was calibrated using the laser excitation wavelength and a saturated sulfate solution; spectra of samples to be directly compared were recorded the same day with no change in experimental geometry. Reported spectra were the result of the averaging of 200 single spectra each recorded with a CCD exposure time of 30 s. Spectral resolution was about 3 cm^{-1}. The band assignments are proposed by analogy with *SW* myoglobin and *Rm*FixL (23, 24).

Band-fitting analyses for the RR and FT-IR data were performed using the GRAMS 32 software. The central frequency values of spectral components in a complex cluster of bands were determined using second derivative and Fourier self-deconvolution. These frequency values and bandwidths of 15 cm^{-1} were used as input parameters for the reiterative band-fitting routine.

RESULTS

UV-Visible Spectroscopy

The UV-visible absorption spectra of the *Bj*FixLH and mutant proteins were recorded in the range 200–800 nm, and the results are summarized in Supplemental Data Table S1. All mutants were able to fully bind CO like the wild-type protein, and the UV-visible data are very similar to that of WT *Bj*FixLH. In contrast, dramatic differences were observed for the mutants in their ability to bind O_2. The formation of a stable Fe-O_2 adduct under similar conditions as WT (10 mM ascorbate, 1 atm O_2) was observed for the R220H, R220I, and R220Q substitutions, whereas the reaction of R220E with dioxygen did not allow formation of any stable adduct; the UV-visible absorption spectra are presented in Fig. 2. The spectrum of WT Fe-O_2 is taken as reference for 100% O_2 fixation (Fig. 2*A*) (18). For R220I and R220Q mutants, the spectra obtained appear as mixtures of Fe^{III}, Fe^{II}, and Fe^{II}-O_2 states, as indicated by shoulders at 395 nm (Fe^{III} species) and 440 nm (Fe^{II} species) for R220I. For each mutant, the contributions of the Fe^{II} deoxy or Fe^{III} Met states were subtracted in order to obtain a homogeneous Soret band similar to that of WT Fe^{II}-O_2. The resulting spectra are presented in Fig. 2, *B* and *C*, and data are reported in Supplemental Data Table S1. The amounts of the oxy form were estimated to be 50 and 80% for the R220I and R220Q mutants, respectively. For the R220H mutant, a 100% of O_2 fixation was observed under 1 atm O_2 as well as under air (20% O_2; data not shown). Thus, this mutant exhibits a higher affinity for O_2 than wild type, since wild type is unable to form 100% of the oxy form under air.

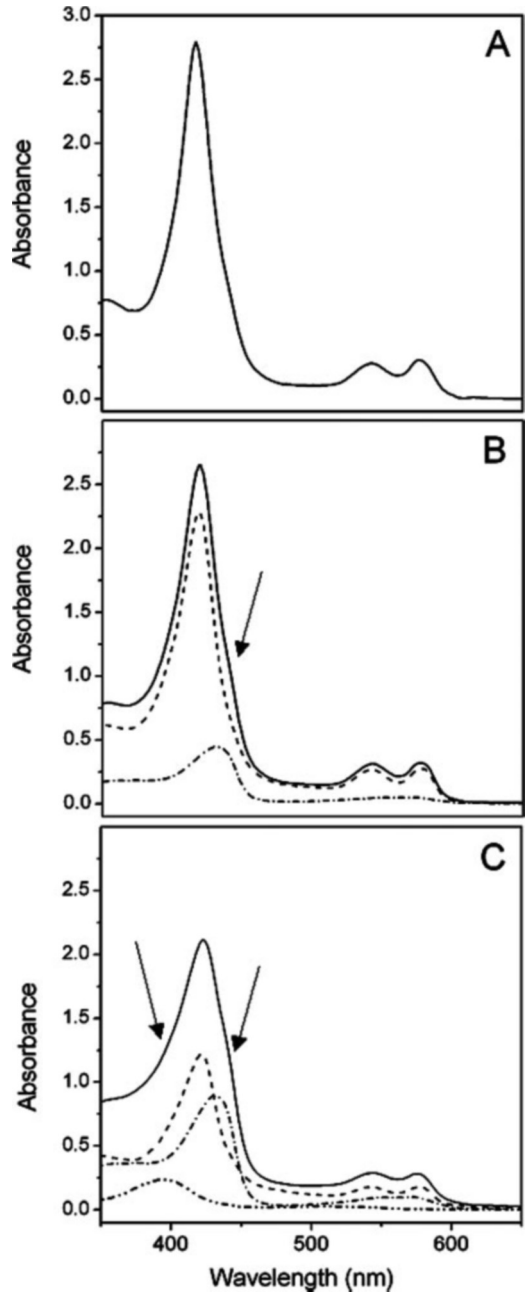

FIG. 2. **UV-visible absorption spectra of *Bj*FixL Fe^{II}-O_2 adducts recorded at ambient temperature for the WT FixL (*A*), the R220Q (*B*), and the R220I (*C*) mutants at pH 7.4.** *Solid line*, solutions after reduction by ascorbate exposed to 1 atm O_2, *arrows* indicate shoulders caused by Fe^{II} or Fe^{III} contributions, (–·–·–) Fe^{II} contribution, (–··–··–) Fe^{III} contribution, (– – – –) resulting Fe^{II}-O_2 spectra obtained by subtracting the Fe^{II} and Fe^{III} contributions. For R220Q, a contribution of 20% Fe^{II} deoxy was subtracted, and the resulting spectrum exhibits a Soret band at 419 nm with an absorbance value corresponding to 77% of that of WT Fe^{II}-O_2. For R220I, contributions of 40% Fe^{II} and 10% Fe^{III} were removed, and the resulting spectrum shows a Soret band at 421 nm with a Soret peak value corresponding to 46% of that of WT $Fe^{II}O_2$.

Oxygen and Carbon Monoxide Binding

FixL proteins have lower O_2 and CO affinities than most natural myoglobins, because of slow ligand association rates as reported in Table I (17). k_{on} values for O_2 binding were measured by flash photolysis of the oxy-adduct as described under "Materials and Methods" (see Supplemental Data Fig. S1). For the R220E mutant a mixed O_2/CO atmosphere experiment was performed (30 μM CO and 1.3 mM O_2); the first phase of the

TABLE I
Kinetics and equilibrium constants for the reaction of ferrous BjFixL with O_2 and CO compared to those of other hemoproteins

Protein	O_2				CO k_{on}	Ref.
	P_{50}	K_d	k_{on}	k_{off}		
	mmHg	*μM*	*X 10^{-4} M^{-1}s^{-1}*	*s^{-1}*	*X 10^{-4} M^{-1}s^{-1}*	
*Bj*FixL	76	140	14.5	20	0.5	17, 27
*Bj*FixLH	18	33	30	10	1.6	This work
R220H *Bj*FixLH	5	9	130	12	11	This work
R220Q *Bj*FixLH	137	250	100	250	7	This work
R220I *Bj*FixLH	1030	1875	160	3000	13	This work
R220E *Bj*FixLH	1200	2140	70	1500	3.7	This work
R220A *Bj*FixL		1500	0.2–0.4	6	1.2	14
R220A *Bj*FixLH	700	1250	140	1750	4.9	This work
*Rm*FixLT	27	0.005	22	11	1.2	17
*Rm*FixL*	17	0.003	22	6.8	1.7	16, 28
*Ec*Dos		340	0.19	0.64	0.081	25
*Ec*DosH		20	3.1	0.61	0.78	25
		13	0.26	0.034	0.11	2
*SW*Mb	0.48	0.91	1700	15	51	26, 33
H64R *SW*Mb		1.1	7900	880	2600	26
H64Q *SW*Mb		5.5	2400	130	100	26
H64I *SW*Mb		7	9000	6400	800	26
H64A *SW*Mb		4.3	5300	2300	420	26
*Pc*Hb	0.45	0.84	3010	25.2	0.8	39
HemAT		0.72	3200	23	0.7	36

rebinding kinetics has a rate that is the sum of $k_{on\,(O2)}$ and $k_{off\,(O2)}$ (see Supplemental Data Fig. S2). After 4 ms, the rebinding reaction under 1 atm O_2 was almost complete, and the ΔA value corresponds to formation of 42% of the oxy-complex for the R220I mutant, 74% for the R220Q mutant, and 100% for the R220H mutant (Fig. 3). The experiment was also performed under air for the R220I mutant, leading to formation of only 10% of the oxy-complex. These results are in full agreement with the UV-visible results presented above.

The results obtained for the heme domain of the wild-type *Bj*FixL protein are compared with those obtained for the wild-type full-length protein (Table I) (17). Truncation of the kinase domain apparently results in the lowering of the $P_{50\,(O2)}$ value. The same observation has been previously made for the *Rm*-FixL protein (17) and the *Ec*DOS sensor (25).

Upon mutation of Arg^{220}, the association rate of O_2 and CO are modified in a similar manner and k_{on} values for both ligands follow the order: WT < R220E < R220Q < R220H < R220I.

The k_{off} values for CO dissociation were calculated from experimentally determined K_{CO} and $k_{on\,(CO)}$ values. A consensus value for $k_{off\,(CO)}$ at 25 °C was about 0.06 ± 0.03 s^{-1}. The k_{off} values for O_2 dissociation given Table I were determined from mixed O_2/CO atmosphere (see "Materials and Methods"). Mutation of Arg^{220} strongly influences the k_{off} rates, which follows the order: R220I ~ R220E < R220Q < R220H ~ WT. k_{off} values are very similar for *SW* Mb and for the R220H *Bj*FixLH mutant (Table I). Replacement of the histidine residue in *SW* Mb and in the R220H *Bj*FixLH mutant by a glutamine or an isoleucine leads to an increase of the k_{off} value for both proteins by a factor of 10–20 or 200–400, respectively. For Mbs in general, increased k_{off} values have been associated with weakening of H-bonding to the bound O_2 molecule (26).

Finally, $P_{50\,(O2)}$ binding coefficient were calculated from the kinetic (on and off) rates and are reported in Table I. The values obtained for the R220I, Gln, and Glu mutants are higher than for the wild-type protein, indicating a lower affinity for dioxygen. This is mainly because of a large increase of the k_{off} value. In contrast, the R220H mutant exhibits a lower $P_{50\,(O2)}$ value, largely because of an increase of the k_{on} value with respect to WT.

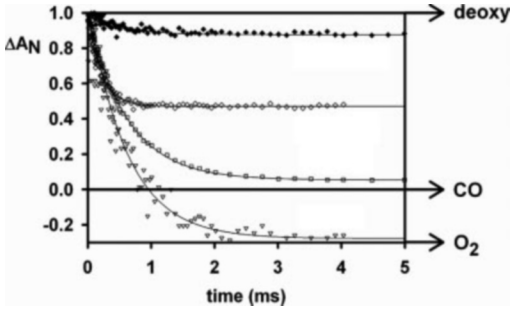

FIG. 3. **O_2 rebinding kinetics measured at pH 7.4 and 25 °C.** The change in absorbance was monitored at 436 nm, after flash photolysis of the CO-complex of the protein under 1 atm of O_2 or under air. R220I under air (◆), R220I under 1 atm O_2 (◇), R220Q under 1 atm O_2 (□), and R220H under 1 atm O_2 (▽). The R220H mutant is fully saturated under 1 atm O_2.

Raman Spectroscopy

Fe^{II}-CO Low Spin 6-Coordinated States—In the *Bj*FixLH ferrous state, CO is known to be a partial inhibitor of the phosphorylation activity of the kinase domain (14). The UV-visible absorption spectra of the Fe^{II}-CO adduct of WT *Bj*-FixLH, and the mutants were almost identical (Supplemental Data Table S1). RR spectra of the Fe^{II}-CO adducts studied here (see Supplemental Data Fig. S3) all exhibit ν_2, ν_3, ν_4, and ν_{10} mode frequencies which clearly indicate that all are indeed in ferrous low spin 6-coordinated states (27). Remarkably, in the high frequency region of the RR spectra, no changes in frequency are observed for the core size sensitive (23) heme modes ν_2 and ν_3 for all mutants as compared with WT, which indicate no significant changes of the heme conformation or core size upon mutation. It is also noted that the oxidation state marker and back-bonding-sensitive ν_4 mode frequency is unaffected by the mutations. Even the CH_2 scissor mode and the $\delta_{C\beta CaCb}$ bending mode of the vinyl substituents, which serve as sensitive probes of the heme environment, observed at 1489 cm^{-1} and 414 cm^{-1} respectively, remain unaffected indicating no significant modification of the heme pocket upon mutation (23).

The Fe-CO moiety is characterized by the $\nu_{Fe\text{-}CO}$ stretching mode found at 500 cm^{-1} for the WT and by the $\nu_{C=O}$ mode seen at 1966 cm^{-1} (Fig. 4) (27). These RR frequencies are similar to those previously reported for *Bj*FixLH (28). They are also very

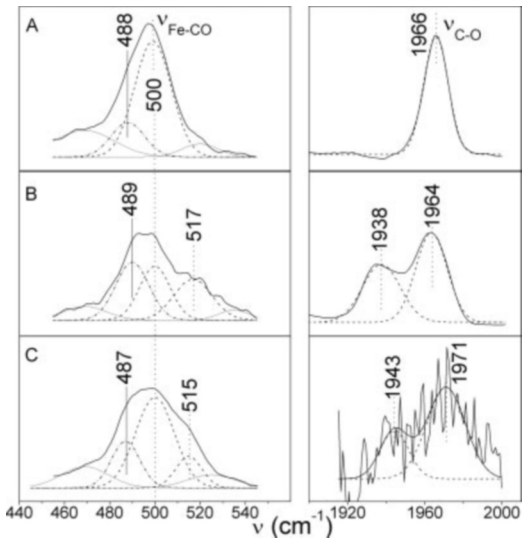

FIG. 4. **Vibrational spectra of the Fe^{II}-CO adduct for the WT protein and the R220H and R220Q mutants.** *A*, WT CO-FixLH; *B*, R220H CO-FixLH; *C*, R220Q CO-FixLH. The low frequency spectra (*left*) were recorded with a resonance Raman spectrometer, whereas the high frequency spectra (*right*) were recorded with a FT-IR spectrometer, except for the R220Q mutant, which was not enough concentrated to allow FT-IR measurements. RR spectra were recorded with λ = 413.1 nm. *Solid line* corresponds to the ν_{Fe-CO} stretching mode band simulation, whereas *dashed line* is attributed to porphyrin contributions at 500/490 cm^{-1} (see Fig. 6).

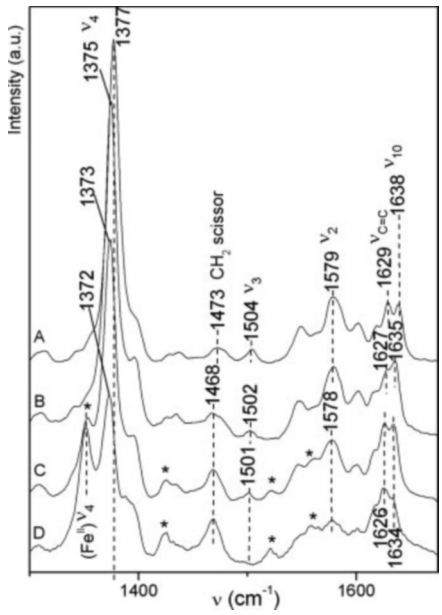

FIG. 5. **High frequency RR spectra (1300–1700 cm^{-1}) of the oxy-*Bj*FixLH forms recorded with λ = 413.1 nm at pH 7.4.** *Asterisk* indicates the Fe^{II} contribution. *A*, $^{16}O_2$ WT FixLH; *B*, $^{16}O_2$ R220H; *C*, $^{16}O_2$ R220Q; *D*, $^{16}O_2$ R220I.

similar to those of Mb at acidic pH values (29) that are reported to arise from an open heme pocket conformation in which CO has little electrostatic interaction with the surrounding amino acids. Thus, our observations indicate an open conformation and an absence of interaction between the CO ligand and the Arg^{220} in FixL, consistent with the x-ray structure of the Fe^{II}-CO adduct, which shows that the Arg^{220} remains outside of the heme distal pocket and pointing toward the heme propionate 7 group, as it does in the Fe^{II} and Fe^{III} states (20).

Lorentzian band fitting analysis (see "Materials and Methods") of the complex 500 cm^{-1} band in the RR spectrum of the WT *Bj*FixLH Fe^{II}-CO adduct (Fig. 4) reveals an intense component at 500 cm^{-1} and a less intense component at 488 cm^{-1}. The majority of the intensity of the 500 cm^{-1} component corresponds to the ν_{Fe-CO} stretching mode (28). We note that RR spectra of the 6-coordinated Fe^{II}-NO (Data not shown and Ref. 28) and Fe^{II}-O_2 adducts (Fig. 6, Ref. 24, 28, 33) all exhibit a weak 500/490 cm^{-1} band, which does not shift upon NO or O_2 isotopic editing. This weak 500/490 cm^{-1} porphyrin mode band is usually not clearly attributed but may be due to ν_{33} and/or γ_{12} modes (23). The 488 cm^{-1} component seen in the band-fitting analysis of the CO adducts is thus ascribed to this underlying weak 500/490 cm^{-1} band.

For both the R220I and R220E mutants, the ν_{Fe-CO} stretching mode frequency is observed at 494 cm^{-1}, a slightly lower frequency but still indicating an open conformation. Thus we conclude that no interaction is present between the CO ligand and Ile^{220} or Glu^{220}.

For the R220H and R220Q mutants, the ν_{Fe-CO} band clearly exhibits a shoulder around 515 cm^{-1} (see Supplemental Data Fig. S3). Both the ν_{Fe-CO} and the $\nu_{C=O}$ bands were analyzed using a Lorentzian band-fitting routine (Fig. 4). The $\nu_{C=O}$ band shows two major components, indicating two conformations for the Fe^{II}-CO adduct. The 1964 and 1971 cm^{-1} frequencies for the R220H and R220Q mutants respectively, are attributed to the open conformation also seen for the WT protein (1966 cm^{-1}). It is therefore associated with the 500 cm^{-1} ν_{Fe-O} band found in the low frequency area. The second contribution is found at 1938 and 1943 cm^{-1} for the R220H and R220Q mutants respectively, indicating a decrease in the C=O bond strength. They are attributed to a second closed conformation where the CO ligand is in interaction (*e.g.* via H-bonding from the protein to the CO ligand) reflecting more $Fe^{\delta+}=C=O^{\delta-}$ electronic character (27). The 1938 and 1943 cm^{-1} frequencies are correlated with the ν_{Fe-CO} components at 515 and 517 cm^{-1}, respectively.

For the closed Fe^{II}-CO conformations in the mutants, the frequencies observed are very similar to those reported for *SW* Mb ($\nu_{C=O}$ = 1947 cm^{-1}) and its H64Q mutant ($\nu_{C=O}$ = 1945 cm^{-1}) (30), and native Elephant Mb (ν_{Fe-CO} = 515 cm^{-1} and $\nu_{C=O}$ = 1984 cm^{-1}) where a Gln residue is present instead of the conserved His(E7) in the distal pocket (31). Thus, we propose that in the second closed conformation observed for the R220H and R220Q mutants of *Bj*FixLH, the CO ligand is interacting with either the His^{220} or the Gln^{220}, respectively. Because these two side chains are capable of donating H-bonds, the interaction is probably a H-bond

The propionate $\delta_{C\beta CcCd}$ bending mode is sensitive to H-bonding and upshifts in frequency when the propionate groups are engaged in such interactions (32). The RR band corresponding to this mode is seen at 385 cm^{-1} for the wild-type FixL protein, but is downshifted by 2 cm^{-1} in the Fe^{II}-CO adducts of all the mutants, reflecting a weakening or rupture in the H-bonding to the propionate 7 (see Supplemental Data Fig. S3). This is fully consistent with the crystallographic structures which indicate one H-bond between Arg^{220} and the propionate 7 group for the Fe^{II}-CO state in the WT protein (20). However, these H-bond ruptures in the mutant CO adducts did not significantly influence the heme conformation as indicated by lack of significant changes in the high frequency core size marker bands and the vinyl modes (see above and Supplemental Data Table S2).

Fe-O_2 States—The RR spectra of the oxygenated (1 atm of O_2 pressure) Fe^{II} *Bj*FixLH from WT, R220H, R220Q, and R220I are presented in Figs. 5 and 6. The high frequency spectra (Fig. 5, 1300–1700 cm^{-1}) of the R220Q and R220I mutants contain contributions from the Fe^{II} deoxy forms, consistent with the reduced affinity for O_2 of the R220Q and R220I mutants deduced from the UV-visible spectra. In the following, only

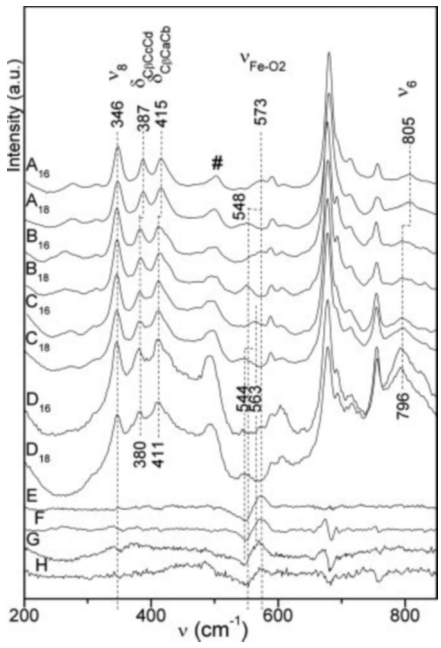

FIG. 6. **Low frequency RR spectra (200–850 cm^{-1}) of the oxy-*Bj*FixLH forms recorded with λ = 413.1 nm at pH 7.4.** #, porphyrin modes around 500/490 cm^{-1}. A_{16}, $^{16}O_2$ WT *Bj*FixLH; A_{18}, $^{18}O_2$ WT *Bj*FixLH, B_{16}, $^{16}O_2$ R220H; B_{18}, $^{18}O_2$ R220H; C_{16}, $^{16}O_2$ R220Q; C_{18}, $^{18}O_2$ R220Q; D_{16}, $^{16}O_2$ R220I; D_{18}, $^{18}O_2$ R220I; *E*, ($^{16}O_2 - {}^{18}O_2$) × 2 WT; *F*, ($^{16}O_2 - {}^{18}O_2$)*2 R220H; *G*, ($^{16}O_2 - {}^{18}O_2$) × 2 R220Q; *H*, ($^{16}O_2 - {}^{18}O_2$) × 2 R220I. For *spectra D*, Raman contributions from the quartz sampling tube are seen as very broad underlying bands centered at ~440 and 810 cm^{-1}.

the salient spectroscopic features of the Fe^{II}-O_2 adduct will be discussed; these are summarized in Supplemental Data Table 2.

An $^{18}O_2$-sensitive band at 573 cm^{-1} was observed in the low frequency WT *Bj*FixLH spectrum (Fig. 6) and attributed to the Fe-O_2 stretching mode, $\nu_{Fe\text{-}O2}$. This frequency is very similar to that reported in another *Bj*FixLH study (28) and to that observed for soluble truncated *Rm*FixL* (571 cm^{-1}) (16). For *SW* myoglobin, a band corresponding to $\nu_{Fe\text{-}O2}$ was seen at 571 cm^{-1} (33). For this latter protein, the terminal O atom of the oxygen ligand is known to be H-bonded to His^{64} and it has been reported that the Fe-O_2 frequency is not sensitive to H-bonding at the terminal O atom (33). When $^{18}O_2$ was used to form the oxy-*Bj*FixLH adduct, the $\nu_{Fe\text{-}O2}$ 573 cm^{-1} band downshifted by 25 cm^{-1} (Fig. 6). An inverse relationship is reported between the ^{18}O isotopic shift of the $\nu_{Fe\text{-}O2}$ modes and the Fe-O-O angle (34). The −25 cm^{-1} ^{18}O isotopic downshift value observed for WT FixLH is slightly smaller than the value for *SW* Mb (Table II) and consistent with a slightly larger Fe-O-O angle for oxy-*Bj*FixLH as seen in the crystallographic structures: 124° for *Bj*FixLH (15) compared with 115° for Mb (33). Consistent with other FixLH resonance Raman data, we were unable to observe a band attributable to the $\nu_{O\text{-}O}$ stretching mode using 413.1 or 406.7 nm excitation into the Soret absorption band (28). For the R220H and R220I mutants, the $\nu_{Fe\text{-}O2}$ mode is also observed at 573 cm^{-1} and the ^{18}O isotopic shift are −25 and −23 cm^{-1}, respectively. The latter value is very similar to that of WT *Bj*FixLH, implying little change in Fe-O-O geometry thus indicating no significant steric modifications upon mutation. The observations for the R220Q mutant are markedly different; the $\nu_{Fe\text{-}O2}$ mode is observed at a significantly lower frequency, 563 cm^{-1}, and the isotopic shift is only −19 cm^{-1}. Low $\nu_{Fe\text{-}O2}$ frequencies have also been previously reported in other heme proteins (Table II). In several hemoglobins, low $\nu_{Fe\text{-}O2}$ frequencies are related to strong H bonds especially with the oxygen atom bound to the iron atom (33, 35, 36). Low $\Delta\nu$ isotopic shifts have been previously related to geometric changes of the bound oxygen and an increase of the Fe-O-O angle (34). For example, *Ec*DOS exhibits a similar low 562 cm^{-1} band (Table II) and its low frequency was rationalized as resulting from a change in Fe-O-O angle induced by steric factors (28).

For our case, using a simple linear triatomic model (34), the −19 cm^{-1} ^{18}O isotopic downshift of the $\nu_{Fe\text{-}O2}$ mode we observe with the R220Q mutant corresponds to a Fe-O-O angle of 155° (37). This angle would thus correspond to a frequency of the $\nu_{Fe\text{-}O2}$ of about 523 cm^{-1}, which is even lower than the observed frequency of 563 cm^{-1}. Therefore it seems unlikely that the lowered $\nu_{Fe\text{-}O2}$ frequency observed for the R220Q mutant is caused by a dramatic change in angle and is more likely due to the presence of an H-bond to the iron-binding oxygen atom, most likely from the introduced amide side chain at position 220. It has been previously reported that the $\nu_{Fe\text{-}O2}$ mode is insensitive to H-bonding interactions at the terminal oxygen atom (29), however, downshifts of ~10 cm^{-1} for this mode have been reported for cases where H-bonds are present on the oxygen atom coordinating the iron atom (38, 39). The RR results for the R220Q mutant are indeed very similar to those reported for the heme-containing signal transducer protein (HemAT) oxygen sensor (Table II), a globin sensor protein where a H-bond to the oxygen atom binding the Fe^{II} atom is present (38). The sensitivity of the $\nu_{Fe\text{-}O2}$ mode to H/D exchange was also examined and compared with the results obtained for WT protein. In the WT protein, the $\nu_{Fe\text{-}O2}$ band downshifts by about 2 cm^{-1} upon hydrogen/deuterium exchange (data not shown). For the R220Q mutant, no downshift was observed indicating that the hydrogen donor does not have readily exchangeable protons. The $\nu_{Fe\text{-}O2}$ frequency as well as its H/D insensitivity are properties similar to those reported for *Pc*Hb, where a glutamine residue is interacting with the iron-bound oxygen atom (Table II) (39). We propose that in the R220Q mutant of *Bj*FixLH the glutamine 220 is H-bonded with the iron-bound oxygen atom (Fig. 7).

In the high frequency region (Fig. 6), the intense 1377 cm^{-1} band for WT exhibits the highest ν_4 frequency observed for the O_2 adducts. This band is seen to downshift by 2 cm^{-1} in the R220H mutant, 4 cm^{-1} in the R220Q and 5 cm^{-1} in R220I; for this latter mutant the ν_4 frequency (1372 cm^{-1}) is similar to that observed for all the mutant CO adducts (1371 cm^{-1}, see Supplemental Data Table S2). The ν_4 mode is predominantly pyrrole C_a-N stretching in character (27). Its frequency serves as an oxidation state marker and is only weakly sensitive to core size, however it is sensitive to the electronic effects of back-bonding from the Fe^{II} dπ orbitals (27). For π acid ligands such as O_2 (and CO and NO) bound to the heme Fe^{II} atom, electron withdrawal to the ligand π^* orbitals via back-bonding competes for back-bonding to the heme π^* orbitals; the ν_4 frequency increases as back-bonding to the π acid ligand increases. From the WT Fe^{II}-O_2 *Bj*FixLH crystal structure it is known that Arg^{220} is in H-bond interaction with the terminal oxygen atom of the O_2 ligand (15). The ν_4 frequency should reflect the strength of the interaction of the distal residue with the oxygen ligand; the greater this interaction, the greater the back-bonding to the O_2 ligand. The ν_4 frequencies observed for the *Bj*FixLH mutants follow the order R220I < R220Q < R220H < WT. The R220I mutant exhibits the lowest ν_4 frequency for the O_2 adducts and indicates the least degree of back-bonding consistent with the fact that the Ile side chain is incapable of donating a H-bond to the O_2 ligand. For the R220Q mutant, the H-bond interaction with the Fe-bound oxygen atom and Gln^{220} as seen in our RR experiments does not appear to strongly modify the back-bonding as its ν_4 frequency

TABLE II
Observed Resonance Raman vibrational frequencies and Soret Absorption Bands for the oxy forms of BjFixL and myoglobin

Protein	λ_{Soret}	ν_4	$\nu_{Fe\text{-}O2}$	$\nu_{Fe\text{-}18O2}$	$\Delta\nu$	H-bond	Ref.
	nm	*cm^{-1}*	*cm^{-1}*	*cm^{-1}*	*cm^{-1}*		
*Bj*FixLH WT	419		569	547	−22		28
	417	1377	573	548	−25	O_T[a]-Arg^{220}	This work
R220H	417	1375	573	544	−25	O_T-His^{220}	This work
R220Q	419	1373	563	544	−19	O_B[b]-Gln^{220}	This work
R220I	421	1372	573	550	−23	None	This work
*Rm*FixL*	417	1376	571	550	−21	Nr[c]	16, 28
*Ec*DosH	417	-	562	538	−24	Nr	28
*SW*Mb WT	417	1377	571	544	−27	O_T-His^{64}(E7)	31, 33
H64L	-	-	570	543	−27	None	33
*Pc*Hb	415	1375	563	540	−23	O_B-Gln(E7) O_T-Tyr(B10)	39
HemAT	414	1372	560	-	-	O_B-X[d]	38

[a] O_T, terminal oxygen atom.
[b] O_B, Fe-bound oxygen atom.
[c] Nr, H-bond not reported.
[d] X, unidentified residue.

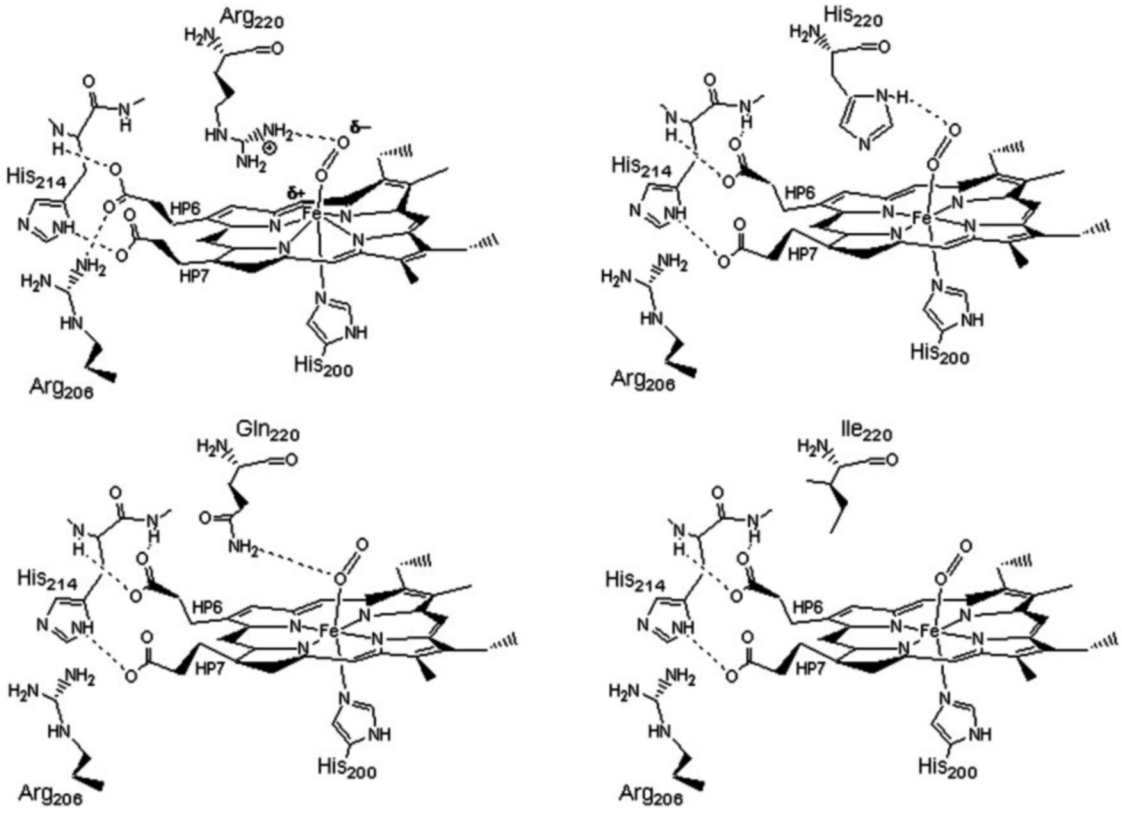

FIG. 7. **Important heme/O_2/protein interactions for the oxy-state of the WT protein and the R220H, R220Q, and R220I mutants based on the resonance Raman studies in this work.** Note the absence of the H-bond between Arg^{206} and propionate 6 in the mutants.

is comparable to that of the R220I mutant. For R220H, the $\nu_{Fe\text{-}O2}$ frequency is identical to those of WT and R220I and not sensitive to H-bond to the terminal oxygen atom (33). However, the ν_4 frequency of 1375 cm^{-1} indicates relatively greater back-bonding for the R220H mutant most likely because of the formation of a H-bond between the terminal oxygen atom and the His^{220}; this H-bonding situation is very similar for most of the myoglobin proteins (26). We notice that the ν_4 frequency is highest for the WT protein. This is fully consistent with formation of a H-bond between the terminal oxygen atom and Arg^{220} (15), and the increase in back-bonding compared with the R220H mutant can be ascribed to the positive charge of Arg^{220} in addition to the H-bond formed.

Changes in the core-size sensitive ν_3 and ν_{10} bands are also observed. This latter band is particularly sensitive to core-size changes; for WT, its frequency is so high that it is now well resolved from the $\nu_{C=C}$ vinyl stretching band (1629 cm^{-1}) and is clearly observed at 1638 cm^{-1}. The elevated frequencies observed for the dioxygen WT adduct are in line with a significantly decreased heme core-size as compared with the WT CO adduct. Thus, the WT *Bj*FixLH-O_2 adduct imparts special structural characteristics to the heme not observed for the other adducts CO and NO (data not shown). Upon Arg^{220} mutation, the ν_3 and ν_{10} bands downshift, although less for the R220H mutant than for the others, reflecting heme core size expansion of the O_2 adducts. Remarkably, these observations are in stark contrast to the insensitivity of these same bands for the mutant CO adducts

(Supplemental Data Fig. S3). This clearly indicates a particular sensitivity of the heme-O_2 adduct structure toward the interaction of Arg^{220} with the O_2 ligand not seen for the other adducts. The intermediate frequencies reported for the R220H mutant indicate that the heme conformation is in between that of WT Fe^{II}-O_2 and that of the R220Q and R220I mutant adducts. We note that the ν_4 frequency discussed above is also somewhat sensitive to heme core size changes, although much less than the ν_3 and ν_{10} bands. Thus, the ν_3 and ν_{10} frequency shifts reported seem to reflect heme conformational changes such as increases in core-size and enhanced back-bonding to O_2 (as discussed below). The WT O_2 adduct exhibits the most back-bonding and the smallest core-size.

Moreover, one other band exhibits a very large downshift for the mutants: the pyrrole breathing mode ν_6 (805 to 796 cm^{-1}) (Fig. 6) (23). Its very high frequency in the WT oxy state indicates a peculiar heme conformation. The lower frequencies for those modes in the mutants are similar to those reported for the Fe^{II}-CO state (Supplemental Data Table S2) where the heme pocket reorganization related to the shift of the FG loop is not observed (20). Therefore, we propose that the ν_6 mode acts as marker bands for the unique heme conformation of the WT oxy-*Bj*FixLH form.

In both, the high and low frequency regions, modes involving the vinyl substituents are downshifted in the mutants, such as the $\nu_{C=C}$ mode (1629 to 1626 cm^{-1}) and the $\delta_{C\beta CaCb}$ mode (415 to 411 cm^{-1}). This suggests changes in the heme conformation or the heme position within the binding pocket between the WT and the mutants in the Fe^{II} oxy states. The $\delta_{C\beta CcCd}$ bending mode of the propionate groups is observed as a single prominent band at 387 cm^{-1}, a value similar to what was previously reported (384 cm^{-1}) (28). As for the Fe^{II}-CO forms, no splitting of this band is observed for the Fe^{II}-O_2 complexes. The same observation was made for *Rm*FixL* (16). The same mode is seen as a single band at 377 cm^{-1} for horse heart MbO_2 (40) and *Pc*HbO_2 (39) and at 378 cm^{-1} for *SW*MbO_2 (31) despite crystallographic structures, which indicate different H-bonding states for the propionate 6 and 7 groups for each protein. Thus our observation of a single band, despite different H-bonding patterns of the two propionate groups in *Bj*FixLH-O_2 as revealed by the crystal structure (15), is consistent with previous Raman observations for similar proteins. According to the FixL crystal structure, binding of O_2 results in the rupture of the Arg^{220}-propionate 7 H-bond and in the formation of a new H-bond between propionate 6 and Arg^{206}. Thus, the relatively high frequency of 387 cm^{-1} reflects that at least one propionate group is involved in a strong H-bond, most likely propionate 6. The sizeable downshift (7 cm^{-1}) of this band upon Arg^{220} replacement, suggests a breaking of this H-bond on the propionate 6 group in the mutants.

DISCUSSION

The data presented here clearly show that arginine 220 strongly influences the level of O_2 binding. For myoglobins, the k_{off} value is dependent on the oxy-complex structure and is lowered by H-bond formation between the bound oxygen molecule and residues in the distal pocket such that at position E7 (native histidine) (33). Mutation of His(E7) in *SW* myoglobin into leucine or other apolar residues not capable of H-bonding leads to a dramatic increase of the k_{off} value whereas the $\nu_{Fe\text{-}O2}$ frequencies are not shifted (26, 33). The k_{off} values (Table I) and the H-bonds to the O_2 ligand in the FixL Fe^{II}-O_2 adducts determined in this work (Table II) are fully consistent with the influence of H-bonding to the O_2 ligand in lowering the k_{off} values seen in the FixL mutants reported here.

For the wild-type *Bj*FixLH protein, the crystallographic structures obtained for the CO and O_2 adducts differ strongly. For the CO adduct, Arg^{220} is in H-bond interaction with the heme propionate 7 (20) and the histidine kinase remains mainly active (14). For the oxy-adduct however, Arg^{220} is pointing inside the heme distal pocket and H-bonded to the oxygen ligand (15). Our Raman results are fully consistent with these observations. Movement of the Arg^{220} together with strong exogenous ligand fixation has been proposed to induce the shift of the FG loop (14, 15, 20), resulting in the inactivation of the histidine kinase domain and structural modifications of the heme pocket responsible for the very high geminate recombination yield observed (18).

For the FixLH Fe^{II}-CO adducts, mutation of Arg^{220} resulted in the loss of the hydrogen bond between propionate 7 and residue 220, as shown in the RR spectra by the downshift of the propionate bending mode $\delta_{C\beta CcCd}$ (Supplemental Data Fig. S3). Moreover, with the histidine and glutamine mutants, our resonance Raman and FT-IR studies indicated a second closed conformation where residue 220 is interacting with the bound CO ligand indicating that residue 220 is pointing toward the heme pocket. Still, the heme conformations deduced from heme core size marker bands in RR appear to be very similar for the wild-type protein and all mutants studied here. Even the frequencies associated with the vinyl substituents (CH_2 scissor mode and $\delta_{C\beta CaCb}$), which are very sensitive to the heme pocket structure, are not influenced by the mutation. These results indicate that there is no correlation between the position of residue 220 inside or outside the heme distal pocket, and the heme core size changes. Thus, disruption of the H-bond between residue 220 and propionate 7 and movement of the Arg^{220} in the wild-type protein does not significantly alter heme conformation and distal pocket. These conclusions suggest that the movement of Arg^{220} into the distal pocket should not be solely responsible for the protein conformational changes associated with kinase deactivation.

For the FixL Fe^{II}-O_2 adducts, mutation of the Arg^{220} leads to a dramatic decrease in the oxygen affinity in all the mutants studied here, except R220H. Decrease of the oxygen affinity is mainly because of a large increase of the k_{off} values for O_2 dissociation. For the R220I mutant of the *Bj*FixLH protein, there is no observed interaction of Ile^{220} with the O_2 ligand, and the k_{off} value for O_2 is increased 300-fold to 3000 s^{-1}. For the R220Q mutant, the Gln^{220} residue is observed to be H-bonded to the Fe-bound oxygen atom of the dioxygen ligand in the oxy state (Fig. 7), as seen from our RR experiments (Fig. 6). This leads to a decrease of the k_{off} value for O_2 dissociation by a factor of 10 compared with the R220I mutant. For both R220I and R220Q mutants, the frequencies of the core-size sensitive modes, namely ν_3 and ν_{10} approach those observed for the CO adduct of *Bj*FixLH (Supplemental Data Table S2), which is known to be far less effective than O_2 in kinase inhibition in the full-length protein. This implies that the heme and/or protein conformational changes leading to kinase inactivity do not occur upon fixation of the O_2 effector molecule in the R220I and R220Q mutants, despite the fact that Gln^{220} is pointing inside the heme pocket and interacts with the bound O_2 molecule.

During the course of our work in this study, very different k_{on} and k_{off} values for O_2 binding and k_{on} for CO binding on the full-length R220A FixL mutant were reported by Dunham *et al.* (14) using different methodologies. These results are also shown in Table I for comparison. Therefore, we constructed the R220A *Bj*FixLH mutant.[2] For the *Bj*FixLH mutants R220I and R220A studied in our work, the k_{on} and k_{off} values are rather comparable and are fully self-consistent with the other mutants in our study. In particular, we obtain a high $k_{off\,(O2)}$ value consistent with the fact that the Ala side chain, like Ile, is not

capable of donating a H-bond to the bound O_2 ligand. The histidine kinase domain is known to influence the binding properties of O_2 in the WT FixL and *Ec*DOS sensors (25); however this effect is not excessively large (compare the first two entries *Bj*FixL and *Bj*FixLH and compare *Ec*DOS with *Ec*DOSH in Table I). Thus, the large differences observed between the $k_{off\,(O2)}$ values for the R220A full-length (6 s^{-1}) and R220A FixLH (1750 s^{-1}) is unexpected and indeed interesting. The origin of this large discrepancy is unknown.

The R220H mutant represents an intermediate between the R220I and R220Q mutants and the WT protein, according to both the k_{off} value for O_2 dissociation and the Raman frequencies of the heme core size marker bands ν_3 and ν_{10}. As for myoglobin, the oxygen binding is stabilized via a H-bond with His^{220} for the FixL mutant studied here (Fig. 7). The ν_4 frequency indicates that this H-bond interaction is stronger than the one reported for the R220Q mutant, consistent with the large decrease of the $k_{off\,(O2)}$ value. The heme core size marker bands are also observed at higher frequencies than for the Ile and Gln mutants. Thus, the strongest interaction between residue 220 and O_2 induces conformational changes, although not for the propionate and vinyl substituents, indicating no major changes in the heme pocket structure. Finally, the structural modifications reported in the R220H mutant are not as important as in the WT protein. The results obtained for the R220H mutants are fully consistent with the conclusion drawn above for the R220Q mutant considering that neither fixation of a strong ligand nor movement of residue 220 by themselves trigger the heme conformational changes. Moreover, the results obtained indicate that formation of a strong hydrogen bond between residue 220 and the terminal oxygen atom is not responsible for the entire heme pocket conformational properties seen in the WT protein.

For the WT protein, the k_{off} value reported for O_2 dissociation is very similar to that reported for the R220H mutant, consistent with a strong hydrogen bond between Arg^{220} and O_2. However, the specific interaction of Arg^{220} with the oxygen ligand enhances the π-acidity of the O_2 ligand compared with the R220H mutant, through the double effect of an H-bond donated by Arg^{220} and the proximity of its positive charge leading to a high degree of back-bonding from iron to O_2 for WT and a very high frequency for the ν_4 mode. This results in a unique heme conformation of the WT oxy-FixLH state with a very small heme core size as indicated by the high frequencies reported for the ν_3 and ν_{10} modes. This probably implies a particular conformation of the heme, where the iron is slightly more out of plane toward O_2 (Fig. 7), together with a particular heme pocket structure as indicated by the very high frequencies reported for the propionate and vinyl bending modes. We especially inferred a strong hydrogen bond network around the propionates, probably because of the interaction of propionate 6 with Arg^{206} reported in the x-ray structure (15). All these structural changes result in the trapping of the O_2 molecule as deduced from geminate recombination experiments (18).

Functional Implications for the FixL-sensing Mechanism—An important new feature revealed in our work, that has implications for the conformational changes in FixL responsible for the functional kinase deactivation, is the observation of significant back-bonding to the oxygen and concomitant core-size changes in the heme.

Enhanced back-bonding toward O_2 should influence the strength of the Fe-His bond which is transaxial to the O_2 ligand, affecting the Fe-His distance. Indeed, for deoxyhemoglobin where the Fe-His stretching mode is easily observed in RR, an inverse linear correlation was observed between the ν_4 electron density marker mode and the Fe-His mode (41). The vibrational frequency and RR band corresponding to the Fe-His mode has not been clearly identified to date for 6-coordinated Fe^{II} hemes (27); however a candidate has been reported to be found at 271 cm^{-1} for oxymyoglobin (42). We have not identified the Fe-His stretching band in our RR spectra of the oxy-adducts.

The reduced core size in WT is not consistent with doming toward the distal side, but it is with the iron coming out of the heme plane toward O_2 (Fig. 7). This should have consequences for the Fe-His distance and geometry.

Given that the His ligand is part of the α-helix that is connected to the critical FG loop (19), the particular O_2 binding properties reported here may participate in signal transduction and ligand discrimination.

CONCLUSION

The results presented in this report clearly demonstrate the importance of the arginine 220 for the binding of O_2 and for ligand discrimination. Arg^{220} plays a crucial role in the signal transduction as discussed above because of its influence on the π acidity properties of O_2. We report a correlation between the heme conformational changes of the *Bj*FixLH protein and the interactions between the bound oxygen and the residue in position 220. Therefore, inhibition of the histidine kinase activity is expected to be lower for the mutants than the WT protein in general agreement with the findings by Dunham *et al.* (14). Our observations strongly suggest that neither fixation of a strong ligand nor displacement of the residue 220 inside the heme pocket are solely responsible for the structural reorganization of the heme. For FixL we propose that an important factor in ligand discrimination is the enhancement of the ligand π acidity by formation of a strong hydrogen-bonding network. The interaction between Arg^{220} and bound O_2 is especially effective because of the double affect of a strong H-bond and proximal positive charge. This leads to a small heme core size, and probably a more out of plane iron atom. These small conformational changes may not be detectable in the x-ray crystal structures. However, displacement of the iron may affect the proximal His^{200}, and therefore the helix containing both the His^{200} and Arg^{206} residues and thereby participate in the heme pocket reorganization responsible for signal transduction.

Acknowledgment—We thank Klara Hola (Ecole Polytechnique) for preparing the R220A FixLH protein.

REFERENCES

1. Gilles-Gonzalez, M-A., Ditta, G. S., and Helinski, D. R. (1991) *Nature* **350,** 170–172
2. Delgado-Nixon, V. M., Gonzalez, G., and Gilles-Gonzalez, M-A. (2000) *Biochemistry* **39,** 2685–2691
3. Chang, A. L., Tuckerman, J. R., Gonzalez, G., Mayer, R., Weinhouse, H., Volman, G., Amikam, D., Benziman, M., and Gilles-Gonzalez M-A. (2001) *Biochemistry* **40,** 3420–3426
4. Denninger, J. W., and Marletta, M. A. (1999) *Biochim. Biophys. Acta* **1411,** 334–350
5. Aono, S., Nakajima, H., Saito, K., and Okada, M. (1996) *Biochem. Biophys. Res. Commun.* **228,** 752–756
6. Shelver, D., Kerby, R. L., He, Y., and Roberts, G. P. (1997) *Proc. Natl. Acad. Sci. U. S. A.* **94,** 11216–11220
7. Dioum, E. M., Rutter, J., Tuckerman, J. R., Gonzalez, G., Gilles-Gonzalez, M-A., and McKnight, S. L. (2002) *Science* **298,** 2385–2387
8. Vreede, J., van der Horst, M. A., Hellingwerf, K. J., Crielaard, W., and van Aalten, D. M. F. (2003) *J. Biol. Chem.* **278,** 18434–18439
9. Safran, M., and Kaelin, W. M., Jr. (2003) *J. Clin. Investig.* **111,** 779–783
10. Sciotti, M-A., Chanfon, A., Hennecke, H., and Fischer, H-M. (2003) *J. Bacteriol.* **185,** 5639–5642
11. Nellen-Anthamatten, D., Rossi, P., Preisig, O., Kullik, I., Babst, M., Fischer, H. M., and Hennecke, H. (1998) *J. Bacteriol.* **180,** 5251–5255
12. Gilles-Gonzalez, M-A., Gonzalez, G., and Perutz, M. F. (1995) *Biochemistry* **34,** 232–236
13. Tuckerman, J. R., Gonzalez, G., Dioum, E. M., and Gilles-Gonzalez, M-A. (2002) *Biochemistry* **41,** 6170–6177
14. Dunham, C. M., Dioum, E. M., Tuckerman, J. R., Gonzalez, G., Scott, W. G., and Gilles-Gonzalez, M-A. (2003) *Biochemistry* **42,** 7701–7708
15. Gong, W., Hao, B., and Chan, M. K. (2000) *Biochemistry* **39,** 3955–3962
16. Tamura, K., Nakamura, H., Tanaka, Y., Oue, S., Tsukamoto, K., Nomura, M.,

Tsuchiya, T., Adachi, S., Takahashi, S., Iizuka, T., and Shiro, Y. (1996) *J. Am. Chem. Soc.* **118,** 9434–9435
17. Gilles-Gonzalez, M. A., Gonzalez, G., Perutz, M. F., Kiger, L., Marden, M. C., and Poyart, C. (1994) *Biochemistry* **33,** 8067–8073
18. Liebl, U., Bouzhir-Sima, L., Négrerie, M., Martin, J-L., and Vos, M. H. (2002) *Proc. Natl. Acad. Sci. U. S. A.* **99,** 12771–12776
19. Gong, W., Hao, B., Mansy, S. S., Gonzalez, G., Gilles-Gonzalez, M-A., and Chan, M. K. (1998) *Proc. Natl. Acad. Sci. U. S. A.* **95,** 15177–15182
20. Hao, B., Isaza, C., Arndt, J., Soltis, M., and Chan, M. K. (2002) *Biochemistry* **41,** 12952–12958
21. Park, H., Suquet, C., Satterlee, J. D., and Kang, C. (2004) *Biochemistry* **43,** 2738–2746
22. Uzan, J., Dewilde, S., Burmester, T., Hankeln, T., Moens, L., Hamdane, D., Marden, M. C., and Kiger, L. (2004) *Biophys. J.* **87,** 1196–1204
23. Hu, S., Smith, K. M., and Spiro, T. G. (1996) *J. Am. Chem. Soc.* **118,** 12638–12646
24. Lukat-Rodgers, G. S., and Rodgers, K. R. (1997) *Biochemistry* **36,** 4178–4187
25. Taguchi, S., Matsui, T., Igarashi, J., Sasakura, Y., Araki, Y., Ito, O., Sugiyama, S., Sagami, I., and Shimizu, T. (2004) *J. Biol. Chem.* **279,** 3340–3347
26. Springer, B. A., Sligar, S. G., Olson, J. S., and Phillips, G. N., Jr. (1994) *Chem. Rev.* **94,** 699–714
27. Spiro, T. G., and Li, X-Y. (1988) in *Biological Applications of Raman Spectroscopy* (Spiro, T. G., ed) Vol. III, pp. 1–37, Wiley Interscience, NY
28. Tomita, T., Gonzalez, G., Chang, A. L., Ikeda-Saito, M., and Gilles-Gonzalez, M-A. (2002) *Biochemistry* **41,** 4819–4826
29. Ramdsen, J., and Spiro, T. G. (1989) *Biochemistry* **28,** 3125–3128
30. Li, T., Quillin, M. L., Phillips, G. N., and Olson, J. S. (1994) *Biochemistry* **33,** 1344–1446
31. Kerr, E. A., Yu, N-T., Bartinicki, D. E., and Mizukami, H. (1985) *J. Biol. Chem.* **260,** 8360–8365
32. Peterson, E. S., Friedman, J. M., Chien, E. Y. T., and Sligar, S. G. (1998) *Biochemistry* **37,** 12301–12319
33. Hirota, S., Li, T., Phillips, G. N., Olson, J. S., Mukai, M., and Kitagawa, T. (1996) *J. Am. Chem. Soc.* **118,** 7845–7846
34. Takahashi, S., Ishikawa, K., Takeuchi, N., Ikeda-Saito, M., Yoshida, T., and Rousseau, D. L. (1995) *J. Am. Chem. Soc.* **117,** 6002–6006
35. Couture, M., Yeh, S-R., Wittenberg, B. A., Wittenberg, J. B., Ouellet, Y., Rousseau, D. L., and Guertin, M. (1999) *Proc. Natl. Acad. Sci. U. S. A.* **96,** 11223–11228
36. Das, T. K., Couture, M., Ouellet, Y., Guertin, M., and Rousseau, D. L. (2001) *Proc. Natl. Acad. Sci. U. S. A.* **98,** 479–484
37. Desbois, A., Momenteau, M., and Lutz, M. (1989) *Inorg. Chem.* **28,** 825–834
38. Aono, S., Kato, T., Matsuki, M., Nakajima, H., Ohta, T., Uchida, T., and Kitagawa, T. (2002) *J. Biol. Chem.* **277,** 13528–13538
39. Das, T. K., Weber, R. E., Dewilde, S., Wittenberg, J. B., Wittenberg, B. A., Yamauchi, K., Van Hauwaert, M-L., Moens, L., and Rousseau, D. L. (2000) *Biochemistry* **39,** 14330–14340
40. Hirota, S., Ogura, T., Appelman, E. H., Shinzawa-Itoh, K., Yoshikawa, S., and Kitagawa, T. (1994) *J. Am. Chem. Soc.* **116,** 10564–10570
41. Rousseau, D. L., and Ondrias, M. R. (1983) *Annu. Rev. Biophys. Bioeng.* **12,** 357–380
42. Walters, M. A., and Spiro, T. G. (1982) *Biochemistry* **21,** 6989–6995